PCCP

Cite this: *Phys. Chem. Chem. Phys.*, 2011, **13**, 9232–9237

www.rsc.org/pccp

PAPER

Electrocatalytic oxidation of nucleobases by TiO_2 nanobelts

Jingjie Cui,[a] Dehui Sun,[a] Weijia Zhou,[a] Hong Liu,*[a] Peiguang Hu,[a] Na Ren,[a] Haiming Qin,[a] Zhen Huang,[b] Jianjian Lin[a] and Houyi Ma[c]

Received 10th January 2011, Accepted 10th March 2011
DOI: 10.1039/c1cp20082h

Two kinds of TiO_2 nanobelts were prepared from commercial P-25 powders *via* an alkaline hydrothermal method with and without an acid etching process. The uncauterized nanobelts (TNs) exhibited a smooth surface, and mixed phases of anatase and TiO_2 (B), whereas the cauterized ones (CTNs) displayed a rough surface and a pure anatase structure. TNs and CTNs were then deposited onto a glassy carbon electrode (GCE) surface with a conductive adhesive (CA), and the resulting chemically modified electrodes exhibited electrocatalytic activities in the oxidation of nucleobases in a 0.1 M phosphate buffer solution (PBS) at pH 7.4. For guanine and adenine, well-defined oxidation peaks were observed in voltammetric measurements at about +0.62 and +0.89 V, respectively, at a potential sweep rate of 100 mV s^{-1}, whereas for cytosine, uracil and thymine, the voltammetric features were not obvious. The average surface coverages (Γ) of guanine and adenine on the CTNs/CA/GCE electrode were estimated to be 4.75×10^{-10} and 7.44×10^{-10} mol cm^{-2}, respectively, which were about twice those at the TNs/CA/GCE electrode. The enhanced activity of the CTN-based electrode towards purine nucleobase oxidation was ascribed to the large specific surface area and anatase structures with enhanced (001) facets of the CTN that facilitated adsorption of the analytes onto the electrode surface and charge transport through the electrode surface layer.

1. Introduction

Quasi-one-dimensional nanobelt materials, in particular metal oxide nanobelts, have attracted great interest because of their unique charge transport properties, which may be exploited for (bio)sensing applications.[1,2] Of these, zinc oxide nanobelts have been examined extensively as active sensing materials.[2,3] However, zinc oxide nanobelts, in general, lack structural stability due to the influence of an array of environmental factors, such as moisture, air and biofluids.[4] In contrast, TiO_2 nanobelts are environmentally stable with unique sensing and biocompatible properties. Therefore, TiO_2 nanobelt-based sensors have become one of the most important research topics in recent years, for instance, in the electrochemical analysis of nucleic acids.

For electrochemical biosensors, the active sensing materials on the electrode act as a catalyst that facilitates the reaction of the biochemical compounds to obtain the output signals.[1] In other words, catalytic activity is a critical element in the selection and development of sensing materials. As there are four polymorphs of TiO_2 (rutile, anatase, brookite and TiO_2 (B)),[5] the properties and performance of TiO_2-based (bio)sensors strongly depend on its crystalline and morphological structure.[6] For instance, anatase TiO_2, with a high percentage of reactive {001} facets, has been found to exhibit the best catalytic activity among these four phases.[7,8] Thus, high purity anatase single-crystal TiO_2 is generally desired for (bio)sensing applications. In addition, it is well-known that low-dimensional nanostructures exhibit efficient charge transport dynamics, a critical component in the function and integration of nanoscale devices.[1] To this end, the fabrication of single-crystal TiO_2 nanobelts represents one of the effective methods to enhance the (bio)sensing performance of TiO_2-based devices.[7] In fact, in a series of earlier studies, we demonstrated gas sensing, antibacterial and photocatalytic applications of single-crystalline one-dimensional TiO_2 nanobelts.[9–14] In the present study, we extend the investigation to the electrochemical oxidation of nucleobases.

The analysis of nucleic acids is critical in a number of areas related to human health, such as the diagnosis of infectious diseases, genetic mutations, drug discovery and food technology.[15] However, conventional techniques for nucleic acid analysis typically require sophisticated and expensive instrumentation and chemical reagents, and/or complex pre-treatments prior to

[a] *State Key Laboratory of Crystal Materials, Center of Bio & Micro/nano Functional Materials, Shandong University, 27 Shandanan Road, Jinan, 250100, P. R. China. E-mail: hongliu@sdu.edu.cn; Fax: +86 053188362807; Tel: +86 053188362807*
[b] *Department of Chemistry, Georgia State University, Atlanta, Georgia, USA*
[c] *Key Laboratory for Colloid and Interface Chemistry of State Education Ministry, Shandong University, Jinan 250100, P. R. China*

testing. In contrast, there are several unique advantages of the electrochemical analysis of nucleic acids, such as fast response, high sensitivity, miniaturized analytical devices, *in situ* environmental monitoring and economic bio-detection, which can satisfy the needs of large-scale genetic testing research.[16] This takes advantage of the electrochemical activities of nucleobases, which were first reported in 1955.[17] Nucleobases consist of five different types of base: adenine (A), guanine (G), cytosine (C), uracil (U) and thymine (T), which may be oxidized or reduced voltammetrically. However, the redox reactions of nucleobases usually occur at very positive or negative potentials,[18,19] where the oxygen and hydrogen evolution reactions from aqueous solutions may compromise the performance of electrochemical analysis. In fact, because of this complication, it has remained a challenge to use electrochemical methods for the analysis of nucleobases.

In addition, because eukaryotic cells regulate the cytoplasmic pH to a narrow range of 7.0 to 7.4 by ion transport with the high buffering capacity of the cytosol,[20,21] in the present study, the electrochemical behaviors of nucleobases were evaluated by using TiO_2 nanobelt-modified electrodes in a PBS buffer solution (pH 7.4). To the best of our knowledge, the electrochemical analysis of nucleobases by using TiO_2 nanobelts as the electrocatalytic material at physiological pH has not yet been reported.

In this study, commercial P-25 powders were used as the precursor and single-crystal TiO_2 nanobelts (TNs) were prepared *via* an alkaline hydrothermal process. Surface-coarsened TiO_2 nanobelts (CTNs) were prepared by using a combined alkaline hydrothermal and acid etching process. The resulting TiO_2 nanobelts (TNs and CTNs) were then employed as the active materials for the electrocatalytic oxidation of nucleobases. The results showed that chemically-functionalized electrodes based on CTNs exhibited enhanced charge transport and surface adsorption of nucleobases, as compared to their TN counterparts, and therefore may serve as a promising material for the electrocatalytic oxidation of nucleobases.

2. Experimental section

2.1 Materials

Titania P-25 (TiO_2, *ca.* 75% anatase and 25% rutile), sodium hydroxide (NaOH), hydrochloric acid (HCl) and sulfuric acid (H_2SO_4) were purchased from China National Medicines Corporation Ltd. Adenine (A), guanine (G), cytosine (C), uracil (U) and thymine (T) were obtained from Aladdin (Shanghai, China). Conductive adhesive was purchased from China Shenzhen Capiton Sci-Technology Co., Ltd. Ultrapurified (Millipore) water was used throughout this study. All reagents were of analytical grade.

2.2 Preparation of TiO_2 nanobelts

Titanate nanobelts were synthesized by a hydrothermal process in a concentrated NaOH aqueous solution. Commercial titania powders (Degussa Co., P-25, a mixture of anatase and rutile in a ratio of 3 : 1) were used as the precursor. Briefly, 0.1 g of the P-25 precursor was mixed with 20 mL of a 10 M NaOH aqueous solution, followed by a hydrothermal treatment at 180 °C in a 25 mL Teflon-lined autoclave for 72 h. The treated powders were washed thoroughly with de-ionized water, followed by a filtration and drying process, affording sodium titanate nanobelts, which were then immersed in a 0.1 M HCl aqueous solution for 24 h and washed thoroughly with water to produce hydrogen titanate nanobelts. These nanobelts were divided into two portions. One part was thermally annealed at 600 °C for 1 h, leading to the formation of TiO_2 nanobelts (TNs). The other part was put into a 25 mL Teflon vessel, which was then filled with a 0.02 M H_2SO_4 aqueous solution up to 80% of the total volume and heated at 100 °C for 12 h. The products were isolated from the solution by centrifugation, washed with de-ionized water several times and then dried at 70 °C for 10 h. The resulting cauterized TiO_2 nanobelts were denoted as CTNs.

2.3 Structure characterization

X-Ray powder diffraction (XRD) patterns of the obtained TiO_2 nanobelts were recorded with a Bruker D8 Avance powder X-ray diffractometer with a Cu-Kα source (λ = 0.15406 nm) at room temperature in the range 2θ = 10 to 70°. The morphologies and size of the TiO_2 samples were examined by using a Hitachi S-4800 field-emission scanning electron microscope (FE-SEM), and the elemental composition was determined by energy dispersive X-ray (EDX) spectroscopy.

2.4 Preparation of TiO_2 nanobelts modified electrodes and electrochemical detection

A glassy carbon electrode (3 mm in diameter) was polished with 0.05 μm α-Al_2O_3 suspensions until a mirror surface was obtained, and rinsed extensively with anhydrous ethanol and de-ionized water. The electrode was then electrochemically cleaned in 0.5 M H_2SO_4 by cycling potentials between −0.3 and +1.8 V at 100 mV s^{-1} until a steady cyclic voltammogram was obtained. A conductive adhesive (CA) was drop-cast onto the cleaned glassy carbon electrode (GCE) surface, onto which 3 μL of an ethanolic suspension of TiO_2 nanobelts (0.5 mg mL^{-1}) was added in a dropwise fashion. After drying, the resulting electrodes were denoted as TNs/CA/GCE or CTNs/CA/GCE.

Electrochemical measurements were performed in a three-electrode configuration. The TiO_2 nanobelts modified electrodes prepared above were used as the working electrode. A Pt foil acted as the auxiliary electrode. All potentials were referred to an Ag/AgCl/KCl saturated reference electrode. All analyte solutions were prepared in 0.1 M PBS (pH 7.4). Voltammetric data were acquired with a CHI 660C electrochemical workstation.

3. Results and discussion

3.1 Characterization of nanobelt structure and composition

Fig. 1 depicts the XRD patterns of the two kinds of TiO_2 nanobelts. It can be seen that for the uncauterized TiO_2 nanobelts (TNs, curve a), in addition to the diffraction features of anatase TiO_2 that are highlighted with asterisks (JCPDS 21-1272), several diffraction peaks of TiO_2 (B) also

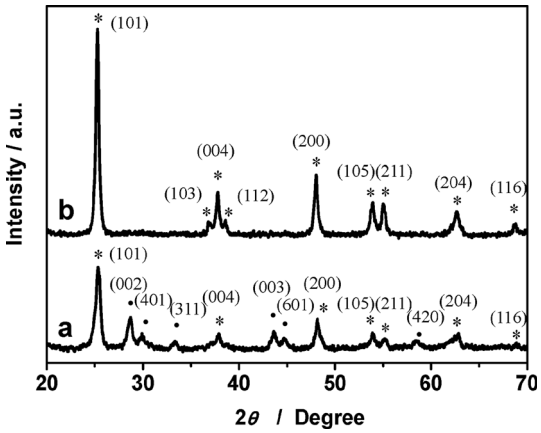

Fig. 1 X-Ray diffraction (XRD) patterns of (a) uncauterized and (b) cauterized TiO_2 nanobelts: (*), anatase TiO_2; (·), monoclinic TiO_2 (B).

appear (denoted with black dots). For instance, the diffraction peaks at 2θ = 28.60, 29.70, 33.32, 43.49, 44.50 and 58.5° can be indexed to the (002), (401), (311), (003), (601) and (420) lattice planes of TiO_2 (B) (JCPDS 46-1238), respectively. This suggests the coexistence of TiO_2 (B) and anatase in the uncauterized TiO_2 nanobelts.[22] For the cauterized TiO_2 nanobelts (CTNs, curve b), only anatase features were observed, with diffraction peaks at 2θ = 25.28, 36.95, 37.80, 38.58, 48.05, 53.89, 55.06, 62.69 and 68.76°, which were ascribed to the (101), (103), (004), (112), (200), (105), (211), (204) and (116) lattice planes of anatase TiO_2 (JCPDS 21-1272), respectively. In addition, in comparison with the diffraction pattern of the TNs, the peaks of the CTNs are sharper, which indicates that the crystallinity of the TiO_2 nanobelts was enhanced markedly after acid etching. For instance, the (004) diffraction peak of the CTNs (curve b) becomes much stronger and sharper than that of the TNs (curve a), suggesting that there are more (001) facets in the resulting anatase crystals.[23] As the (001) facet exhibits a high reactivity in comparison to the others,[7] this suggests that the (electro)catalytic activity of TiO_2 nanobelts may be enhanced simply by the acid etching process, as detailed below.

The morphologies and microstructures of the TiO_2 nanobelts were then investigated by FESEM. Fig. 2 shows a representative SEM micrograph for the (a) uncauterized and (b) cauterized TiO_2 nanobelts. Both samples exhibit a width of 50 to 200 nm, and length up to hundreds of micrometres. The uncauterized nanobelts (TNs, panel a) showed a smooth surface, whereas a rough surface was observed for the cauterized ones (CTNs, panel b), with the surface decorated with TiO_2 nanoparticles of about 20 nm in diameter. Typically, TiO_2 nanobelts grow along the (101) plane. That is, the long axis of the nanobelts is along the [001] direction, with a lack of (001) facets, as observed in Fig. 1a with the uncauterized TiO_2 nanobelts.[24,25] In contrast, after acid treatment, the nanobelt surfaces were roughened and decorated with a number of TiO_2 nanoparticles, such that the effective concentration of the (001) facets was increased drastically, as manifested in the XRD measurements (Fig. 1b). Additionally, energy dispersive X-ray (EDX) analysis showed that the TiO_2 nanobelts (TNs and CTNs)

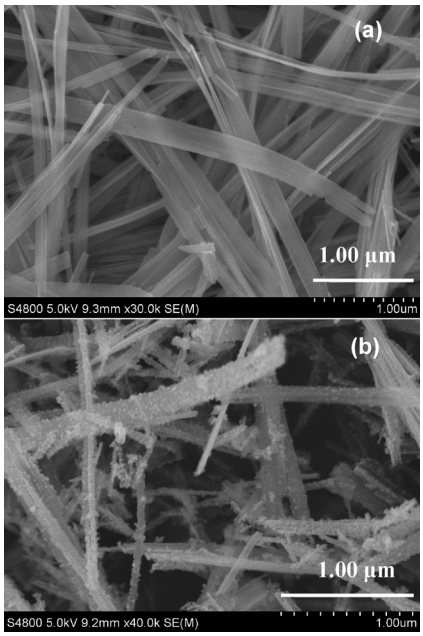

Fig. 2 Representative SEM micrographs of (a) uncauterized and (b) cauterized TiO_2 nanobelts. Scale bars are both 1 μm.

were only composed of Ti and O elements in an atomic ratio close to 1 : 2 (data not shown).

3.2 Electrocatalytic oxidation of nucleobases at TiO_2 nanobelts modified electrodes

The TiO_2 nanobelts obtained above were then used for the electrochemical oxidation of nucleobases by depositing them onto a glassy carbon electrode. Fig. 3 shows the cyclic voltammograms of the TiO_2 nanobelt-modified electrodes in 0.1 M PBS (pH 7.4) in the presence of 0.1 mM guanine and adenine. It can be seen that at the TNs/CA/GCE electrode, whereas the control experiment in a blank PBS supporting electrolyte manifested only a featureless voltammetric profile between +0.5 and +1.2 V, two irreversible oxidation peaks appeared at +0.62 and +0.89 V in the presence of 0.1 mM guanine and adenine. Similar features were observed with the CTNs/CA/GCE electrode. The first peak can be ascribed to the electrooxidation of guanine and the second one to

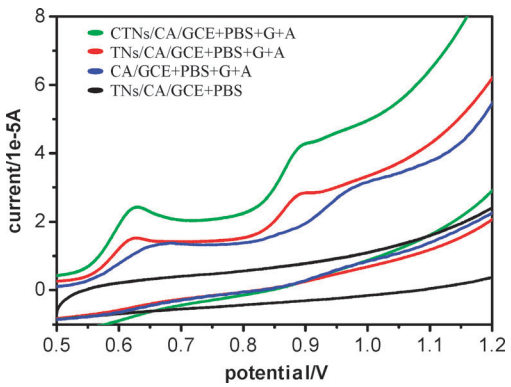

Fig. 3 Cyclic voltammograms of varied chemically-modified electrodes in 0.1 M PBS (pH 7.4) without and with 0.1 mM guanine (G) and adenine (A). Potential sweep rate 100 mV s^{-1}.

adenine.[26] Note that these peak potentials are about 60 and 90 mV more negative than those (+0.68 and +0.98 V) at the CA/GCE electrode, indicative of the catalytic activity of TiO_2 nanobelts toward the oxidation of nucleobases. In addition, the fact that the voltammetric peaks at both TNs/CA/GCE and CTNs/CA/GCE are much sharper than those at CA/GCE suggests that the electron transfer kinetics were markedly enhanced by the incorporation of TiO_2 nanobelts into the electrode surface layer. Also, from Fig. 3, it can be seen that the voltammetric peak currents decrease in the order CTNs/CA/GCE > TNs/CA/GCE > CA/GCE. That is, the CTNs/CA/GCE electrode showed the highest catalytic activity for the electrooxidation of nucleobases. This is likely to be due to the pure anatase crystal structure of the cauterized TiO_2 nanobelts which feature high specific surface areas and (001) facets, as manifested in the XRD and SEM measurements (Fig. 1 and Fig. 2).[7]

Generally, the oxidation of guanine and adenine follows a two-step mechanism involving the total loss of $4e^-$ and a three-step mechanism involving the total loss of $6e^-$.[27,28] These processes will cause mutagenic lesions due to reactive oxygen species, including hydroxyl radicals, and consequently base damage in DNA.[29–31] In aqueous electrolytes, TiO_2 nanobelts as an electrocatalyst electrochemically generate reactive oxygen species, including hydroxyl radicals at the TiO_2 surface.[32] It is most likely that this process facilitates the electrocatalytic oxidation of nucleobases.

Interestingly, the oxidation peak currents of guanine and adenine increase linearly with potential scan rate at both TNs/CA/GCE and CTNs/CA/GCE electrodes, as depicted respectively in Fig. 4 and Fig. 5 (panels (a) and (b)). This suggests that the oxidation of nucleobases is primarily controlled by surface-adsorbed species. For an irreversible surface process, the relationship between oxidation peak current (i_p) and surface coverage (Γ) is[33]

$$i_p = n(1-\alpha)n_\alpha AF^2 v\Gamma/2.718RT \qquad (1)$$

where v is the potential scan rate, R the gas constant (8.314 J mol^{-1} K), T the absolute temperature (T = 298 K), F the Faraday constant (96 485 C mol^{-1}), A the geometrical area of the working electrode (A = 0.07 cm^2), n the total number of electrons involved in the oxidation of guanine or adenine ($n_{guanine}$ = 4, $n_{adenine}$ = 6),[27,34] n_α the number of electrons involved in the rate-determining step and α the electron transfer coefficient, which can be determined by the linear dependence of the oxidation peak potential ($E_{P,a}$) with the logarithm of the potential scan rate (v),[33,35]

$$E_{p,a} = E^\circ - (RT/(1-\alpha)nF)\ln(RTk_s/(1-\alpha)nF) + (RT/(1-\alpha)n_\alpha F)\ln v \qquad (2)$$

where E° is the formal potential and k_s is the standard rate constant of the surface reaction. In the potential range examined, the plots of $E_{p,a}$ *vs.* ln$v$ were linear for both the TNs/CA/GCE and (d) CTNs/CA/GCE electrodes, as manifested in panels (c) of Fig. 4 and Fig. 5. Linear regressions show that for guanine oxidation at the TNs/CA/GCE and CTNs/CA/GCE electrodes, $(1-\alpha)n_\alpha$ was estimated to be 1.2339 and 1.1999, respectively, whereas for adenine oxidation, 0.7309 and 0.8137. Thus, by assuming a flat electrode surface, the average surface coverage (Γ) of guanine at the TNs/CA/GCE and CTNs/CA/GCE electrodes can be estimated to be about 2.868×10^{-10} and 4.750×10^{-10} mol cm^{-2}, respectively, whereas for adenine, 5.677×10^{-10} and 7.438×10^{-10} mol cm^{-2}. It can be seen that the surface concentration of nucleobases was higher on CTNs/CA/GCE than on TNs/CA/GCE, which might be accounted for by the enhancement of the specific surface area of the acid treated nanobelts.[36]

Consistent behaviors were observed in square wave voltammetric (SWV) measurements.[37] Fig. 6 shows the SWVs of varied chemically-modified electrodes in the presence of 0.1 mM guanine and adenine, or cytosine, uracil and thymine. In the presence of thymine, uracil (or cytosine), at the CA/GCE (curve a) electrode, only a featureless profile was observed, signifying the lack of activity of the electrode. In contrast, at the TNs/CA/GCE (curve b) and CTNs/CA/GCE (curve c) electrodes, two weak and broad oxidation peaks appeared at +1.1 and +1.25 V, which are again attributed to the electrocatalytic oxidation of the pyrimidine bases. In comparison with the voltammetric responses of the purine bases (curves d and e), the peak currents of the pyrimidine bases are much lower and the oxidation potentials are far more positive, most probably because of their sluggish electron transfer kinetics.[38] This may be accounted for by the lower aromaticity of pyrimidines, where electron deficiency renders it more difficult to oxidize pyrimidines than purines.[39]

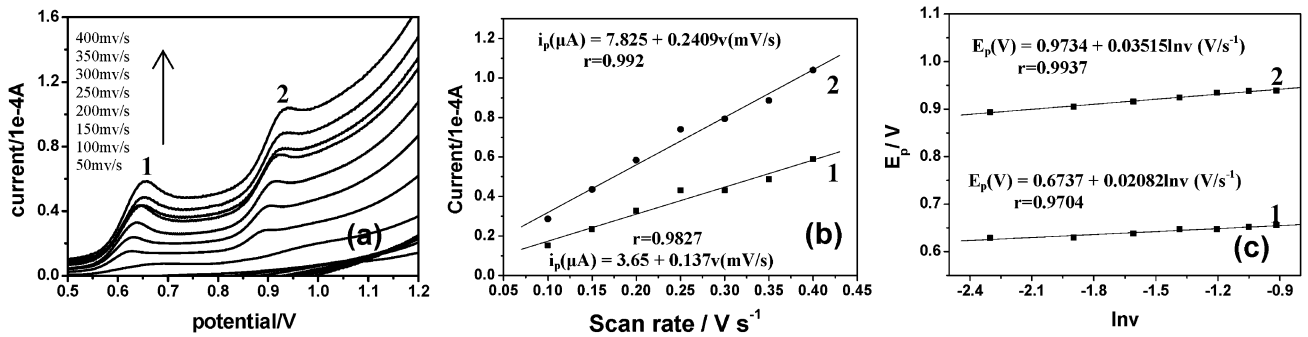

Fig. 4 (a) Cyclic voltammograms at different scan rates; (b) variation of peak currents with potential scan rates; and (c) variation of peak potentials (E_p) with the logarithm of the potential scan rate (ln$v$) in 0.1 M PBS (pH 7.4) with 0.1 mM guanine (1) and adenine (2) at the TNs/CA/GCE electrode.

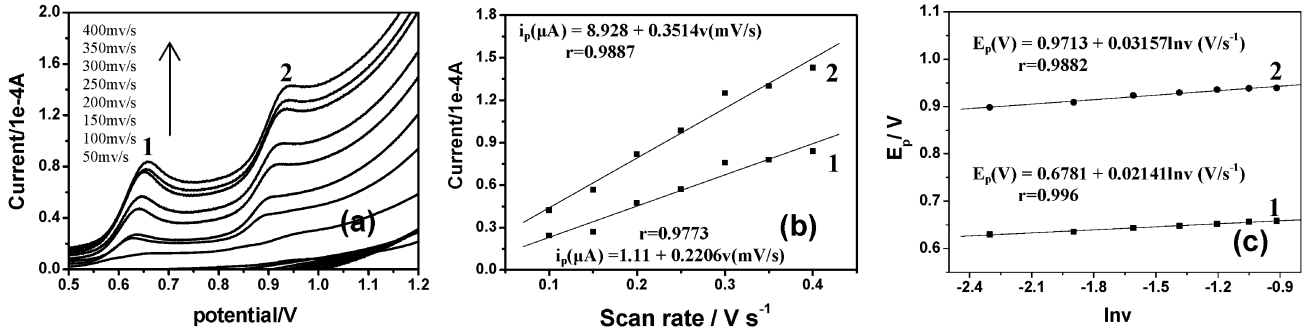

Fig. 5 (a) Cyclic voltammograms at different scan rates; (b) variation of peak currents with potential scan rates; and (c) variation of peak potentials (E_p) with the logarithm of the potential scan rate (ln$v$) in 0.1 M PBS (pH 7.4) with 0.1 mM guanine (1) and adenine (2) at the CTNs/CA/GCE electrode.

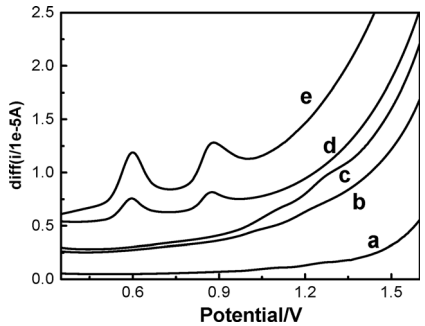

Fig. 6 Square wave voltammograms (SWVs) at (a) CA/GCE, (b) TNs/CA/GCE and (c) CTNs/CA/GCE in 0.1 M PBS (pH 7.4) containing 0.1 mM thymine, uracil (or cytosine); and (d) TNs/CA/GCE and (e) CTNs/CA/GCE in 0.1 M PBS (pH 7.4) containing 0.1 mM guanine and 0.1 mM adenine. Frequency 5 Hz, potential amplitude 25 mV and step potential 4 mV.

4. Conclusions

TiO_2 nanobelts have been successfully prepared from commercial P-25 powders *via* an alkaline hydrothermal process, and surface-coarsened TiO_2 nanobelts were obtained *via* an acid etching process. The uncauterized TiO_2 nanobelts (TNs) exhibited a smooth surface and mixed phases of TiO_2 (B) and anatase, whereas the cauterized TiO_2 nanobelts (CTNs) showed a rough surface and a pure anatase structure with enhanced (001) facets. Both TiO_2 nanobelts (TNs and CTNs) were then deposited onto a glassy carbon electrode for the electrooxidation of nucleobases in 0.1 M phosphate buffer solution (PBS) at pH 7.4. The results indicated that the nanobelt-functionalized electrodes exhibited a markedly enhanced electrocatalytic activity in the oxidation of purine nucleobases as compared to the pyrimidine ones. Importantly, the electrocatalytic activity was found to be manipulated by the surface and crystalline structures of the TiO_2 nanobelts, where the electron transport and surface adsorption properties were varied. These results suggest that TiO_2 nanobelts may serve as promising active materials in the electrochemical oxidation of nucleobases.

Acknowledgements

This research was supported by the NSFC (NSFDYS: 50925205, Grant: 50990303, 50872070, 50702031 IRG: 51021062), the Independent Innovation Foundation of Shandong University (2009JC011) and the Program of Introducing Talents of Disciplines to Universities in China (111 program no. b06017).

References

1 U. Yogeswaran and S. M. Chen, *Sensors*, 2008, **8**, 290–313.
2 Z. L. Wang, *Annu. Rev. Phys. Chem.*, 2004, **55**, 159–96.
3 Z. L. Wang, *ACS Nano*, 2008, **2**, 1987–1992.
4 J. Zhou, N. S. Xu and Z. L. Wang, *Adv. Mater.*, 2006, **18**, 2432–2435.
5 J. F. Banfield and D. R. Veblen, *Am. Mineral.*, 1992, **77**, 545–557.
6 W. J. Zhou, H. Liu, R. I. Boughton, G. J. Du, J. J. Lin, J. Y. Wang and D. Liu, *J. Mater. Chem.*, 2010, **20**, 5993–6008.
7 H. G. Yang, C. H. Sun, S. Z. Qiao, J. Zou, G. Liu, S. C. Smith, H. M. Cheng and G. Q. Lu, *Nature*, 2008, **453**, 638–642.
8 K. Yanagisawa and J. Ovenstone, *J. Phys. Chem. B*, 1999, **103**, 7781–7787.
9 Y. M. Wang, G. J. Du, H. Liu, D. Liu, S. B. Qin, N. Wang, C. G. Hu, X. T. Tao, J. Jiao, J. Y. Wang and Z. L. Wang, *Adv. Funct. Mater.*, 2008, **18**, 1–7.
10 W. J. Zhou, H. Liu, J. Y. Wang, D. Liu, G. J. Du and J. J. Cui, *ACS Appl. Mater. Interfaces*, 2010, **2**, 2385–2392.
11 L. G. Gai, G. J. Du, Z. Y. Zuo, Y. M. Wang, D. Liu and H. Liu, *J. Phys. Chem. C*, 2009, **113**, 7610–7615.
12 Y. M. Wang, G. J. Du, H. Liu, D. Liu, S. B. Qin, J. Y. Wang, X. T. Tao, M. H. Jiang and Z. L. Wang, *J. Nanosci. Nanotechnol.*, 2009, **9**, 2119–2123.
13 P. G. Hu, G. J. Du, W. J. Zhou, J. J. Cui, J. J. Lin, H. Liu, D. Liu, J. Y. Wang and S. W. Chen, *ACS Appl. Mater. Interfaces*, 2010, **2**, 3263–3269.
14 W. J. Zhou, H. Liu, J. Y. Wang, D. Liu, G. J. Du, S. J. Han, J. J. Lin and R. J. Wang, *Phys. Chem. Chem. Phys.*, 2010, **12**, 15119–15123.
15 O. Pänke, A. Kirbs and F. Lisdat, *Biosens. Bioelectron.*, 2007, **22**, 2656–2662.
16 J. Wang, *Anal. Chim. Acta*, 2002, **469**, 63–71.
17 O. Manousek and P. Zuman, *Collect. Czech. Chem. Commun.*, 1955, **20**, 1340–1352.
18 L. Trnková, J. Friml and O. Dračka, *Bioelectrochemistry*, 2001, **54**, 131–136.
19 M. Fojta, L. Havran, R. Kizek, S. Billova and E. Palecek, *Biosens. Bioelectron.*, 2004, **20**, 985–994.
20 T. J. Povsic and P. B. Dervan, *J. Am. Chem. Soc.*, 1989, **111**, 3059–3061.
21 I. H. Madshus, *Biochem. J.*, 1988, **250**, 1–8.
22 S. S. Chen, Y. H. Zhu, W. Li, W. J. Liu, L. C. Li, Z. H. Yang, C. Liu, W. J. Yao, X. H. Lu and X. Feng, *Chin. J. Catal.*, 2010, **31**, 605–614.
23 X. B. Chen and S. S. Mao, *Chem. Rev.*, 2007, **107**, 2891–2959.
24 D. J. Yang, H. W. Liu, Z. F. Zheng, Y. Yuan, J. C. Zhao, E. R. Waclawik, X. B. Ke and H. Y. Zhu, *J. Am. Chem. Soc.*, 2009, **131**, 17885–17893.
25 H. G. Yang and H. C. Zeng, *J. Am. Chem. Soc.*, 2005, **127**, 270–278.

26 H. Y. Liu, G. F. Wang, D. L. Chen, W. Zhang, C. J. Li and B. Fang, *Sens. Actuators, B*, 2008, **128**, 414–421.
27 Z. H. Wang, S. F. Xiao and Y. Chen, *J. Electroanal. Chem.*, 2006, **589**, 237–242.
28 A. M. Oliveira Brett, J. A. P. Piedade and S. H. P. Serrano, *Electroanalysis*, 2000, **12**, 969–973.
29 D. Wang, D. A. Kreutzer and J. M. Essigmann, *Mutat. Res., Fundam. Mol. Mech. Mutagen.*, 1998, **400**, 99–115.
30 J. Llano and L. A. Eriksson, *Phys. Chem. Chem. Phys.*, 2004, **6**, 4707–4713.
31 A. Klungland, I. Rosewell, S. Hollenbach, E. Larsen, G. Daly, B. Epe, E. Seeberg, T. Lindahl and D. E. Barnes, *Proc. Natl. Acad. Sci. U. S. A.*, 1999, **96**, 13300–13305.
32 L. Jörissen, *J. Power Sources*, 2006, **155**, 23–32.
33 A. J. Bard and L. R. Faulkner, *Electrochemical Methods: Fundamentals and Applications*, John Wiley & Sons, New York, USA, 2001, pp. 236–594.
34 N. de-los-Santos-Álvarez, P. de-los-Santos-Álvarez, M. J. Lobo-Castañón, R. López, A. J. Miranda-Ordieres and P. Tuñón-Blanco, *Electrochem. Commun.*, 2007, **9**, 1862–1866.
35 E. Laviron, *J. Electroanal. Chem.*, 1974, **52**, 355–393.
36 M. Woodson and J. Liu, *Phys. Chem. Chem. Phys.*, 2007, **9**, 207–225.
37 S. P. Kounaves, *Voltammetric Techniques*, Prentice-Hall, Englewood Cliffs, NJ, USA, 1997, ch. 37, pp. 719–720.
38 A. Bose and S. Basu, *J. Lumin.*, 2009, **129**, 1385–1389.
39 P. Cysewski, *J. Mol. Struct.*, 2005, **714**, 29–34.